Optical Engineering

SPIEDigitalLibrary.org/oe

Full Stokes polarimetric imaging using a single ferroelectric liquid crystal device

Luc Gendre
Alban Foulonneau
Laurent Bigué

SPIE

Full Stokes polarimetric imaging using a single ferroelectric liquid crystal device

Luc Gendre
Alban Foulonneau
Laurent Bigué
Université de Haute Alsace
Laboratoire MIPS
Ecole Nationale Supérieure d'Ingénieurs Sud Alsace
12 rue des frères Lumière 68093
Mulhouse Cédex France
Email: laurent.bigue@uha.fr

Abstract. This paper reports the design and the implementation of a Stokes imaging polarimeter able to provide full polarimetric information at 200 fps. This portable implementation is based on a division-of-time architecture and uses a single ferroelectric liquid crystal device as the polarization modulating element. Our system is designed to work at 532 nm with natural light or with controlled illumination, without temperature control. We propose an optimized driving scheme of the modulator such that the liquid crystal device can produce four polarization states which makes it possible to retrieve the full polarimetric information. The modulator characterization is reported and experimental results are provided.
[DOI: 10.1117/1.3570665]

Subject terms: Stokes polarimetry; imaging; liquid crystals; ferroelectrics.

Paper 100894SSPR received Oct. 30, 2010; revised manuscript received Feb. 9, 2011; accepted for publication Mar. 2, 2011; published online Jun. 14, 2011.

1 Introduction

Whereas polarimetry basics[1] have been incepted since the mid-19th century and polarimetric imaging[2,3] was proposed in the 1970s, no imaging implementation able to capture dynamic phenomena was reported until the early 1990s[4]. It probably explains the reduced interest in imaging polarimetry, whereas polarization information, whether Stokes or Mueller information proves to be of interest in many fields such as chemistry, astronomy, atmospheric science, and medicine and proves to be an efficient analysis tool for many applications. Several architectures were proposed including division-of-time polarimeters, division-of-amplitude polarimeters[5,6] and division-of-wavefront systems[7]. The two latter solutions require either a complex optical setup or a very specialized component hard to manufacture. On the contrary, division-of-time polarimeters using liquid crystal (LC) cells are consistent alternatives to more classical architectures, since LC devices tend to be more and more widespread and exhibit high quality. They were reported in several fields ranging from robotic vision[8] to astronomy[9] and today several commercial implementations are available. Nevertheless these implementations still run at reduced frame rates, approximately at a few tens of fps. High-speed LC-based implementations able to estimate the full polarimetric information were reported, but they require at least two LC devices. In this paper, the aim is to design and implement a high-speed portable imaging polarimeter system, possibly low-cost, able to provide the full polarimetric information. A system based on a single analog ferroelectric LC device may be a solution, in terms of speed, simplicity, and cost. We already reported an implementation providing only partial Stokes information (i.e., about linear polarization)[10] and propose in the following an extension of this work in order to retrieve the full polarimetric information.

After a brief description of liquid crystal polarization state analyzers in Sec. 2, Sec. 3 describes the characterization of a tunable ferroelectric liquid crystal modulator. Then Sec. 4 describes the implementation of an imaging polarimeter using a single liquid crystal cell and provides experimental results. Section 5 discusses possible improvements.

2 Polarization State Analysis Using Liquid Crystals

Polarization phenomena have been deeply studied by physicists for at least 300 years, but the first mathematical formalism was proposed by Stokes in 1852[1]. Stokes proposed to gather the entire polarimetric information into a 4-element vector $\mathbf{S} = [s_0\ s_1\ s_2\ s_3]^T$, now named Stokes vector. For the sake of simplicity or speed, many optical setups only provide partial Stokes information, which comes down neither to estimate the angle of polarization nor the circular polarization. In this paper our intention is to provide both a simple setup and to estimate the full polarimetric information. To do so, we implement a polarization state analyzer (PSA) using a single ferroelectric liquid crystal cell and a fixed linear polarizer. Due to its birefringent properties, the LC cell acts as an electrically addressable polarization modulator. Usually LC modulators are supposed to either tune the orientation of their fast axis or their retardance, except twisted-nematic LC cells[11], but the latter are known to operate at a reduced frame rate. Classically, using a single modulator leads to a partial Stokes estimation and two modulators are used [9,12,13]. In this paper, we implement a PSA using a ferroelectric LC cell used in an unconventional manner. Such a cell, whose birefringence Δn evolves as in Eq. (1),[14] is classically used at its design wavelength λ_0 where its fast axis orientation can be tuned at a very high speed.

$$\Delta n(\lambda) \cdot d = \frac{\lambda_0}{2} + C \cdot d \cdot \left(\frac{1}{\lambda^2} - \frac{1}{\lambda_0^2} \right), \tag{1}$$

where d is the LC cell thickness and C is a LC dependent constant.

If this LC cell is used away from its design wavelength λ_0, the intensity measured at the output of the PSA writes:

$$I(\theta,\varphi) = \frac{1}{2}\{s_0 + [\cos^2(2\theta) + \sin^2(2\theta)\cdot\cos(\varphi)]\cdot s_1 + \cos(2\theta)\cdot\sin(2\theta)\cdot[1-\cos(\varphi)]\cdot s_2 - \sin(2\theta)\cdot\sin(\varphi)\cdot s_3\}, \quad (2)$$

where θ is the orientation of the LC cell fast-axis and φ its retardance. Gathering several intensities I for several (θ_i, φ_i) configurations —actually, we should write for several voltage controls V_i— leads to estimate $\mathbf{S}$ as:

$$\mathbf{S} = \mathbf{A}^{-1}\cdot\begin{pmatrix} I(\theta_1,\varphi_1) \\ I(\theta_2,\varphi_2) \\ \vdots \\ I(\theta_i,\varphi_i) \\ \vdots \\ I(\theta_N,\varphi_N) \end{pmatrix}, \quad (3)$$

where $\mathbf{A}$, often referred to as the system matrix, writes :

$$\mathbf{A} = \frac{1}{2}\cdot\begin{bmatrix} 1 & \cos^2(2\theta_1)+\sin^2(2\theta_1)\cdot\cos(\varphi_1) & \cos(2\theta_1)\cdot\sin(2\theta_1)\cdot[1-\cos(\varphi_1)] & -\sin(2\theta_1)\cdot\sin(\varphi_1) \\ 1 & \cos^2(2\theta_2)+\sin^2(2\theta_2)\cdot\cos(\varphi_2) & \cos(2\theta_2)\cdot\sin(2\theta_2)\cdot[1-\cos(\varphi_2)] & -\sin(2\theta_2)\cdot\sin(\varphi_2) \\ \vdots & \vdots & \vdots & \vdots \\ 1 & \cos^2(2\theta_i)+\sin^2(2\theta_i)\cdot\cos(\varphi_i) & \cos(2\theta_i)\cdot\sin(2\theta_i)\cdot[1-\cos(\varphi_i)] & -\sin(2\theta_i)\cdot\sin(\varphi_i) \\ \vdots & \vdots & \vdots & \vdots \\ 1 & \cos^2(2\theta_N)+\sin^2(2\theta_N)\cdot\cos(\varphi_N) & \cos(2\theta_N)\cdot\sin(2\theta_N)\cdot[1-\cos(\varphi_N) & -\sin(2\theta_N)\cdot\sin(\varphi_N) \end{bmatrix}. \quad (4)$$

$\mathbf{A}^{-1}$ is often referred to as the data reduction matrix (DRM). Actually, if $N > 4$ measurements are performed, $\mathbf{A}$ is not square and its pseudo-inverse must be used instead of $\mathbf{A}^{-1}$.

Classically, the ferroelectric LC cell is operated at its design wavelength λ_0 which comes down to replace φ with π, therefore rank ($\mathbf{A}$) is only 3. On the contrary, for instance using λ=532 nm instead of λ_0=633 nm comes down to use a $\lambda/1.68$ plate instead of a $\lambda/2$ plate. Therefore, the fourth column of $\mathbf{A}$ becomes nonzero and with a non-trivial choice of control voltages, rank ($\mathbf{A}$) is 4.

3 Characterization of a tunable ferroelectric liquid crystal modulator

3.1 *Principle*

Our modulator, manufactured by Boulder Nonlinear Systems, Inc., is composed of a ferroelectric liquid crystal (FLC) cell and a linear polarizer. It is supposed to be used as a bistable rotator at 633 nm, but we successfully used it in a tunable manner.[10] As mentioned in Sec. 2 we want to get a modulator that is not a pure rotator and now work at 532 nm. The FLC cell is modeled as a plate with an orientation angle θ and a retardance φ. Its polarization characteristics are analyzed according to the principle exposed in Sec. 2, and the general form of its system matrix is presented in Eq. (4). The usual way to determine the system matrix is to operate a Mueller characterization of the FLC cell at first and then combine it with the Mueller matrix of a linear polarizer in order to obtain the Mueller matrix of the whole PSA. From this last matrix the system matrix would be deduced. However, the FLC cell and the linear polarizer of our modulator are not separable one from the other. Therefore, a conventional Mueller characterization of the FLC cell is impossible. To identify the system matrix, the following Stokes vectors are input to the modulator while controlled by a voltage V:

$$\mathbf{S_0} = \begin{pmatrix}1\\1\\0\\0\end{pmatrix} \quad \mathbf{S}_{\pi/2} = \begin{pmatrix}1\\-1\\0\\0\end{pmatrix} \quad \mathbf{S}_{\pi/4} = \begin{pmatrix}1\\0\\1\\0\end{pmatrix}$$

$$\mathbf{S}_{3\pi/4} = \begin{pmatrix}1\\0\\-1\\0\end{pmatrix} \quad \mathbf{S_r} = \begin{pmatrix}1\\0\\0\\1\end{pmatrix} \quad \mathbf{S_l} = \begin{pmatrix}1\\0\\0\\-1\end{pmatrix}. \quad (5)$$

Measuring the intensity of the output light beam for each of the six Stokes vectors leads to the following equations:

$$\begin{cases} I_0 = \frac{1}{2}[1+\cos^2(2\theta)+\sin^2(2\theta)\cdot\cos(\varphi)] & \text{for input } \mathbf{S_0} \\ I_{\pi/2} = \frac{1}{2}[1-\cos^2(2\theta)-\sin^2(2\theta)\cdot\cos(\varphi)] & \text{for input } \mathbf{S}_{\pi/2} \\ I_{\pi/4} = \frac{1}{2}[1+\cos(2\theta)\cdot\sin(2\theta)\cdot(1-\cos(\varphi))] & \text{for input } \mathbf{S}_{\pi/4} \\ I_{3\pi/4} = \frac{1}{2}[1-\cos(2\theta)\cdot\sin(2\theta)\cdot(1-\cos(\varphi))] & \text{for input } \mathbf{S}_{3\pi/4} \\ I_r = \frac{1}{2}[1-\sin(2\theta)\cdot\sin(\varphi)] & \text{for input } \mathbf{S_r} \\ I_l = \frac{1}{2}[1+\sin(2\theta)\cdot\sin(\varphi)] & \text{for input } \mathbf{S_l} \end{cases}. \quad (6)$$

From this system can be deduced the orientation and the retardance, Eqs. (7) and (8), used to compute the system matrix Eq. (4).

$$\tan(2\theta) = \frac{I_{\pi/2} - I_0 + 1}{I_{\pi/4} - I_{3\pi/4}}, \tag{7}$$

$$\tan(\varphi) = \pm \frac{\sqrt{(I_l - I_r)^2 + \left(\frac{(I_{\pi/4} - I_{3\pi/4})(I_l - I_r)}{1 + I_{\pi/2} - I_0}\right)^2}}{\frac{(I_l - I_r)^2}{1 + I_{\pi/2} - I_0} - 1}. \tag{8}$$

In practice, in order to avoid model approximations, such as assuming that there is no depolarization for example, the system matrix is computed directly from measured intensities, without estimating the orientation angle or the retardance. In other words, we consider that the system matrix writes

$$\mathbf{A} = \frac{1}{2} \cdot \begin{bmatrix} A(V_1) & B(V_1) & C(V_1) & D(V_1) \\ A(V_2) & B(V_2) & C(V_2) & D(V_2) \\ A(V_3) & B(V_3) & C(V_3) & D(V_3) \\ A(V_4) & B(V_4) & C(V_4) & D(V_4) \end{bmatrix}, \tag{9}$$

Which leadsto the following intensity system:

$$\begin{cases} I_0(V) = \frac{1}{2}[A(V) + B(V)] & \text{for } \mathbf{S_0} \\ I_{\pi/2}(V) = \frac{1}{2}[A(V) - B(V)] & \text{for } \mathbf{S_{\pi/2}} \\ I_{\pi/4}(V) = \frac{1}{2}[A(V) + C(V)] & \text{for } \mathbf{S_{\pi/4}} \\ I_{3\pi/4}(V) = \frac{1}{2}[A(V) - C(V)] & \text{for } \mathbf{S_{3\pi/4}} \\ I_r(V) = \frac{1}{2}[A(V) + D(V)] & \text{for } \mathbf{S_r} \\ I_s(V) = \frac{1}{2}[A(V) - D(V)] & \text{for } \mathbf{S_l} \end{cases}. \tag{10}$$

Therefore the system matrix is deduced from the intensity measurements according to the following equation:

$$\mathbf{A} = \frac{1}{2} \begin{bmatrix} I_0(V_1) + I_{\pi/2}(V_1) & I_0(V_1) - I_{\pi/2}(V_1) & I_{\pi/4}(V_1) - I_{3\pi/4}(V_1) & I_r(V_1) - I_s(V_1) \\ I_0(V_2) + I_{\pi/2}(V_2) & I_0(V_2) - I_{\pi/2}(V_2) & I_{\pi/4}(V_2) - I_{3\pi/4}(V_2) & I_r(V_2) - I_s(V_2) \\ I_0(V_3) + I_{\pi/2}(V_3) & I_0(V_3) - I_{\pi/2}(V_3) & I_{\pi/4}(V_3) - I_{3\pi/4}(V_3) & I_r(V_3) - I_s(V_3) \\ I_0(V_4) + I_{\pi/2}(V_4) & I_0(V_4) - I_{\pi/2}(V_4) & I_{\pi/4}(V_4) - I_{3\pi/4}(V_4) & I_r(V_4) - I_s(V_4) \end{bmatrix}. \tag{11}$$

$\mathbf{A}^{-1}$ is obtained by numerical inversion of $\mathbf{A}$.

3.2 *Experimental Characterization*

The bench presented in Fig. 1 is used to characterize the modulator. A Nd:YAG laser produces a beam at 532 nm, enlarged by a beam expander. The static linear polarizer P_1 defines the polarization in input to the rotating set ($\lambda/2$, $\lambda/4$) that generates the elementary Stokes vectors mentioned in Eq. (5). These vectors go through the modulator composed of the FLC cell and a linear polarizer. The light intensity is finally measured by a photodetector.

A typical control signal used for characterization at 100 Hz is depicted Fig. 2. It is globally dc-balanced in order not to damage the FLC cell. It consists of a square signal at 100 Hz (duty cycle 50%), with an amplitude of V_i corresponding to the two voltages $-V_i$ and $+V_i$, and of a transient pulse ($\pm$10 V, width 200 μs) which fastens the modulator response. For the characterization phase, amplitude value V_i will vary from 0 to 5 V with a step of 0.01 V.

Measured intensities versus control voltage for each Stokes vector in Eq. (5) are presented in Fig. 3. From these intensities the orientation angle θ and the retardance φ, depicted Fig. 4 can be deduced. The curves show that the global behavior of the FLC cell is different from that of a half-wave plate, which allows full polarization to be analyzed.

We choose an operating scheme with $N = 4$ measurements. Therefore, four voltages have to be determined. As explained in Sec. 3.1, the system matrix is not evaluated from the angle and retardance estimation, but directly from intensity measurements, according to Eq. (11). In order to determine the more suitable set of amplitudes to control the

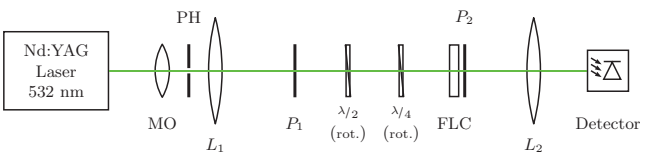

Fig. 1 Setup for partial Mueller characterization of the FLC device. Microscope Objective (MO), Pin Hole (PH), Lenses (L_1 and L_2), static linear polarizers oriented at 0° (P_1 and P_2), rotating half-wave plate ($\lambda/2$), rotating quarter-wave plate ($\lambda/4$), FLC.

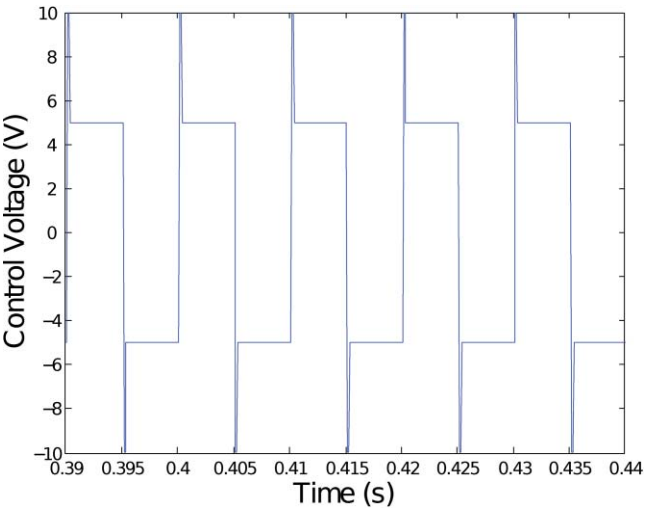

Fig. 2 Control signal used for modulator characterization.

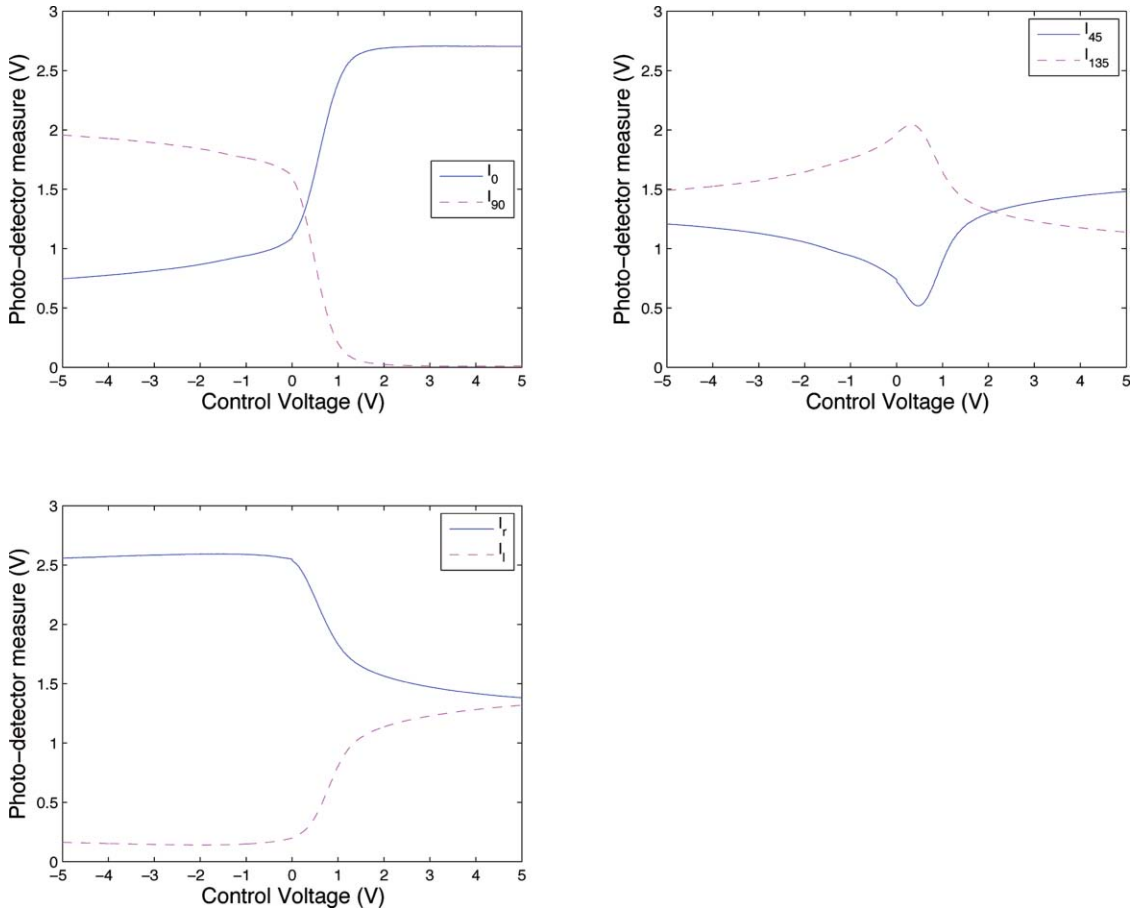

Fig. 3 Intensities measured versus voltage during modulator characterization.

modulator, the condition number (CN) of the system matrix is evaluated for every set $(-V_1, +V_1, -V_2, +V_2)$, where V_1 and V_2 vary from 0 to 5 V. The result[15] is depicted in Fig. 5. The absolute minimum gives the best suitable set of voltages, which corresponds to the voltage set (− 5 V, + 5 V, − 1.27 V, + 1.27 V) for a CN of 37.5.

This first characterization gives information in order to determine the voltage neighborhoods in which looking for the voltages V_1 and V_2. As explained in previous work,[10] further adjustments have to be made on the values of the voltages since the modulator is nonlinear and behaves differently during the characterization (two-level signal) and the final operation (four-level signal). Our signal is finally composed of the voltage set (− 5 V, + 5 V, − 0.9 V, + 0.9 V), which in practice changes the CN to 36.2. The DRM of our system is then computed with these voltages.

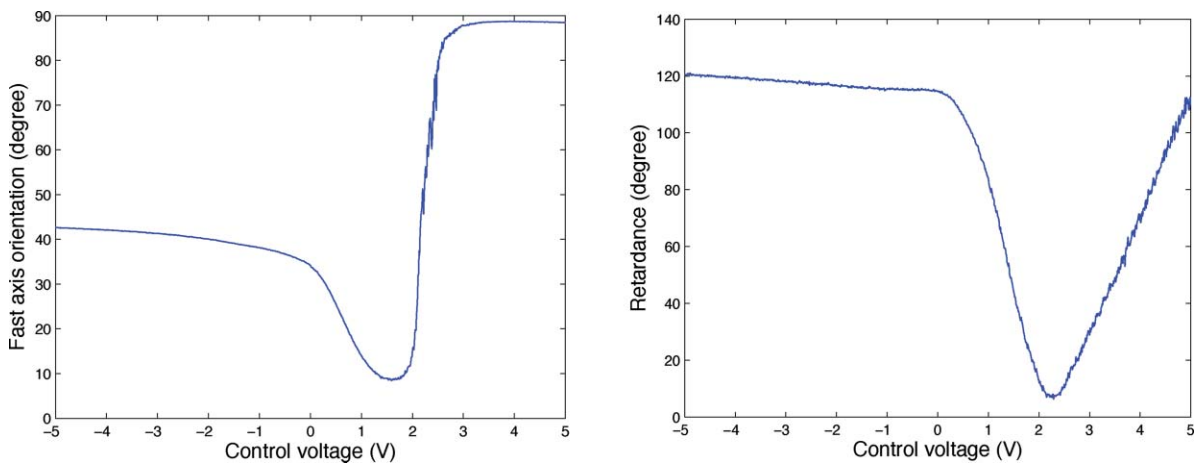

Fig. 4 FLC fast-axis orientation (left) and retardance (right) deduced from intensities versus voltage at 532 nm.

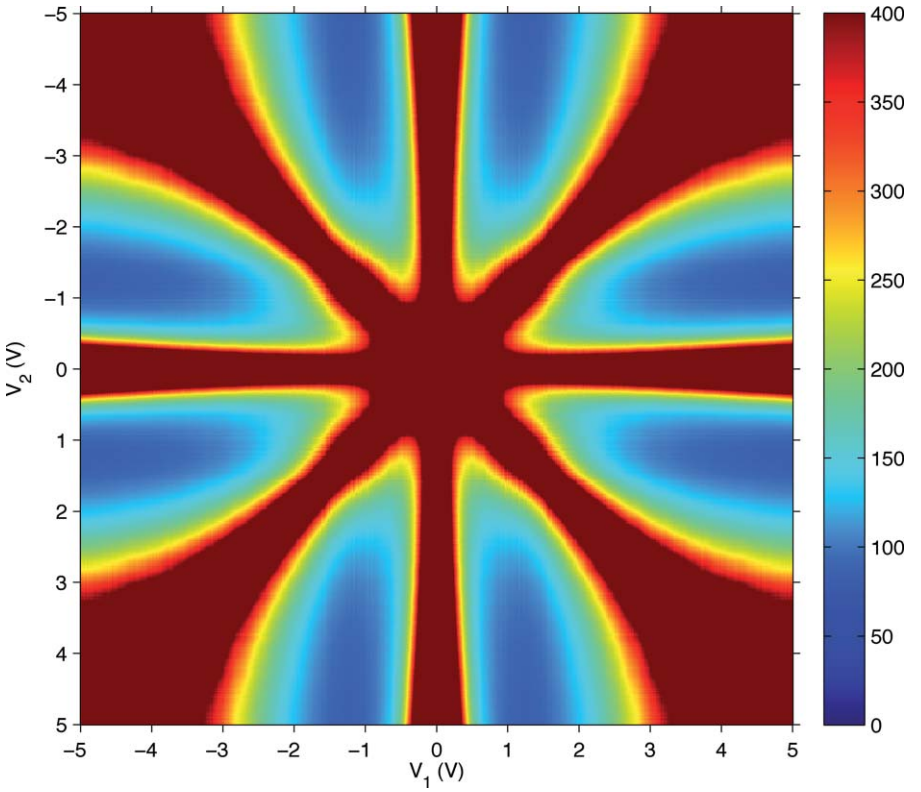

Fig. 5 Condition number for voltage set $(-V_1, -V_2, +V_2, +V_1)$.

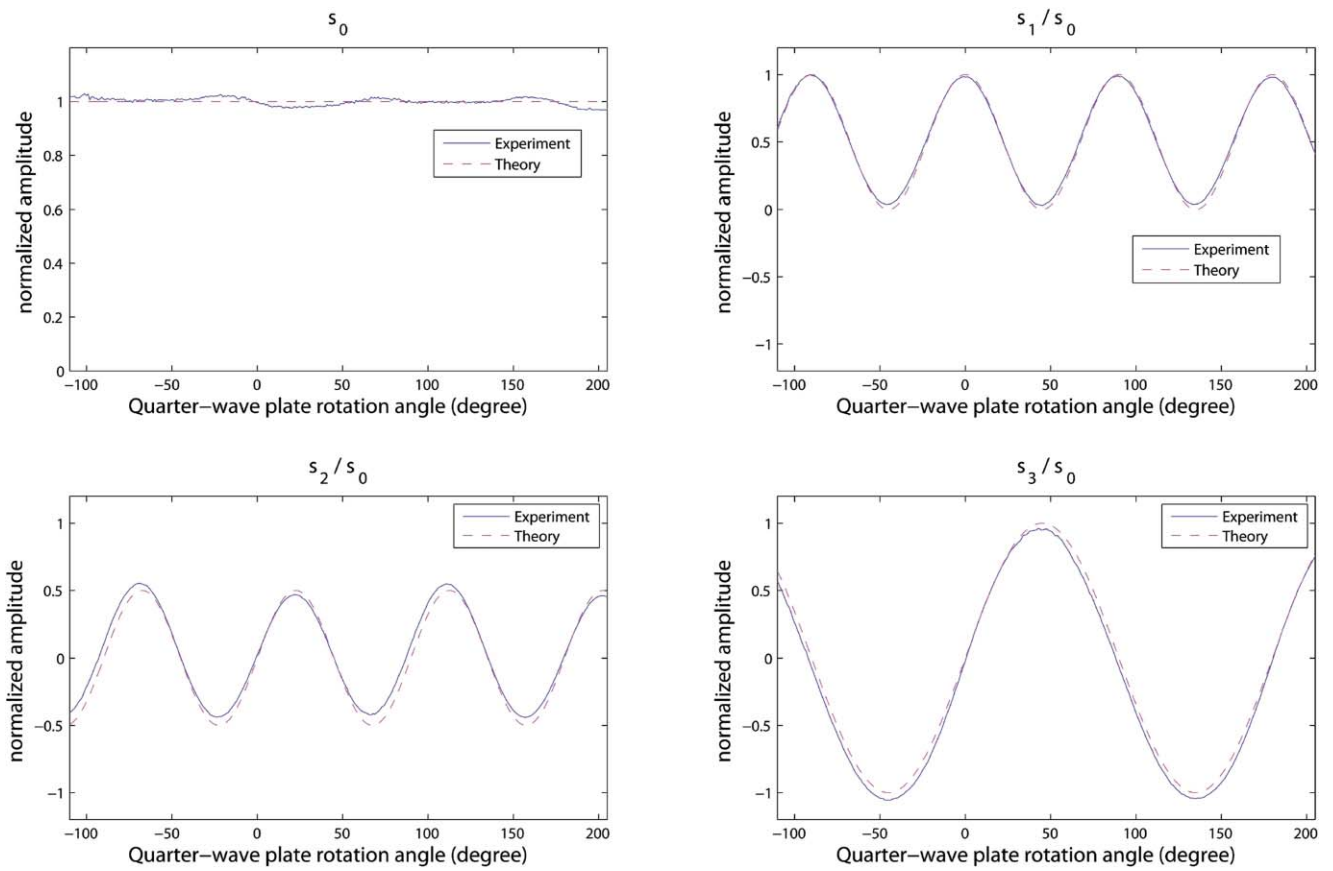

Fig. 6 Stokes vector estimation versus theoretical values.

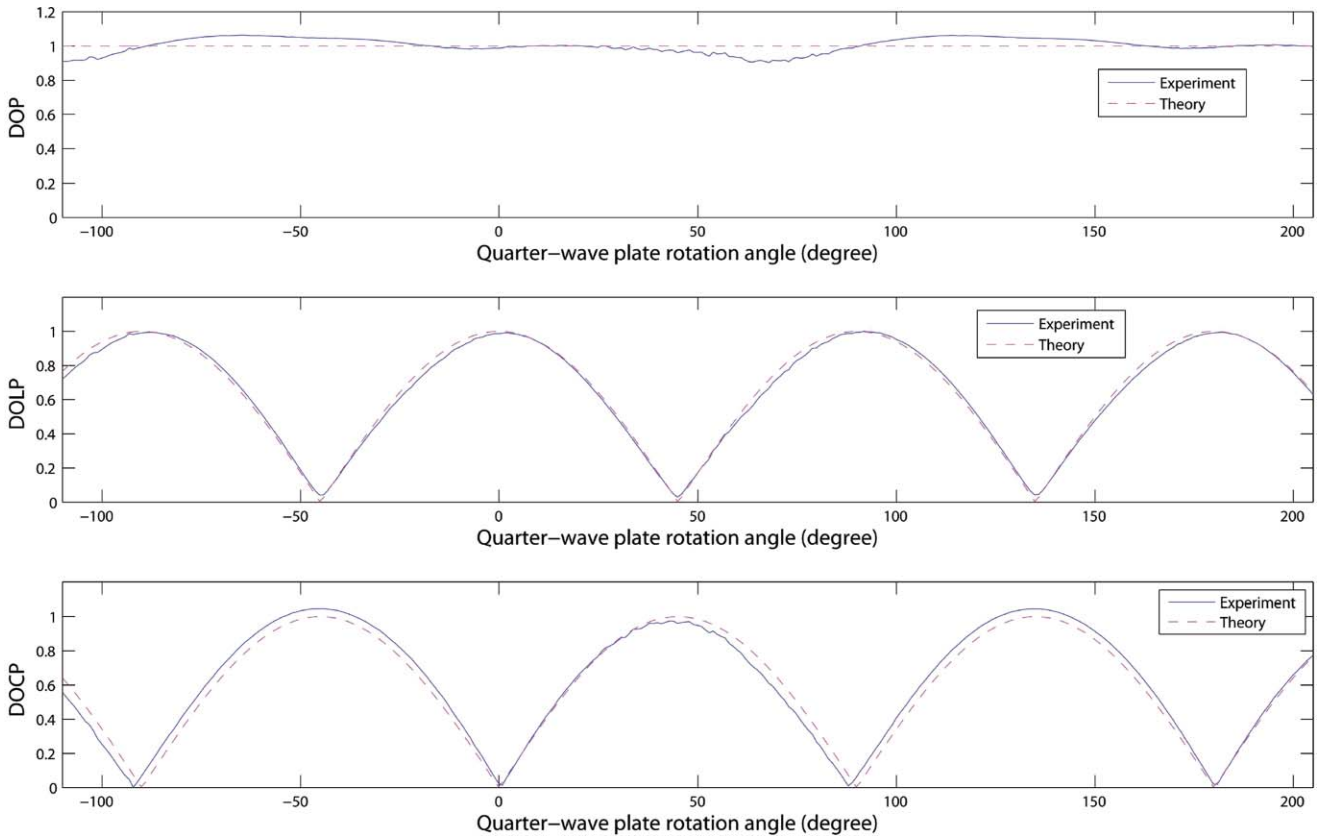

Fig. 7 Experimental and theoretical values for DOP, DOLP, and DOCP versus $\lambda/4$ plate fast-axis orientation.

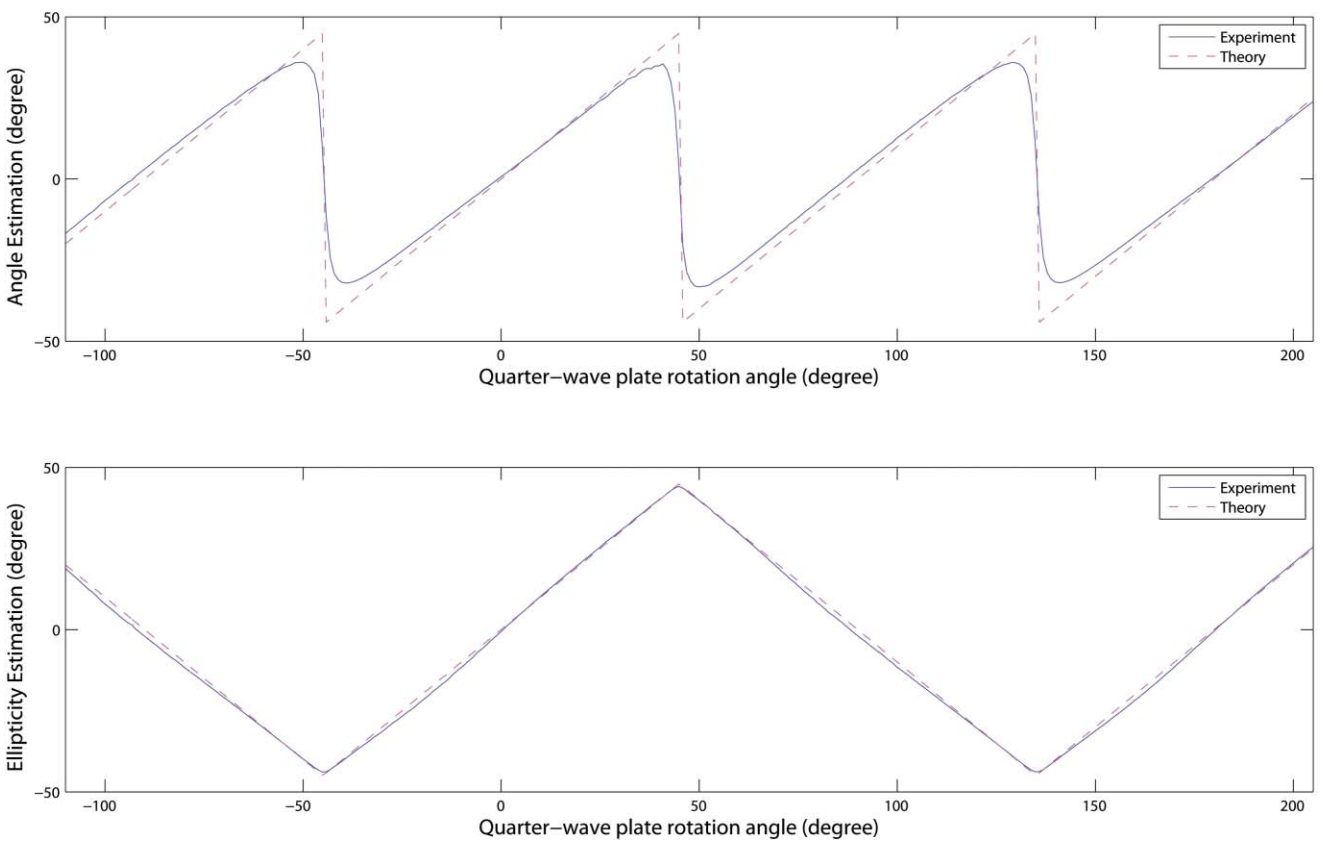

Fig. 8 Experimental and theoretical values for orientation angle ψ and ellipticity ε versus $\lambda/4$ plate fast-axis orientation.

4 Implementation of a Single Ferroelectric Liquid Crystal Modulator as a Stokes Polarization State Analyzer

The modulator is now driven by the final control signal and is used as a PSA. A new polarization state is displayed on the modulator every 5 ms. As a consequence, the polarization is analyzed at 200 fps. The results presented are obtained from raw data, neither with any averaging nor postprocessing.

4.1 *Non-Imaging Validation*

The setup is the same as that presented in Fig. 1. The half-wave plate is static and the quarter-wave plate rotates along the available angular range of the rotating stage with a 1 deg step. Intensities are measured for every position of the quarter-wave plate and from these intensities, Stokes parameters are evaluated using Eq. (3) and using the DRM established in Sec. 3. Results are presented in Fig. 6. In order to minimize laser fluctuations, we use normalized parameters. Stokes parameters evolve in good accordance with expectations. Error on s_0 is within 2.9%, on s_1 within 3.2%, while s_2 and s_3 are, respectively, estimated with a maximum error of 15.9% and 5.7%. Errors may be due to plate imperfections, an inaccurate mounting of the plate in the setup, or to imprecisions in the modulator characterization. Such phenomena are observable on the s_0 component that should theoretically be constant.

From this Stokes vector estimation, other figures can be evaluated. Figure 7 shows the evaluation of the degree of polarization (DOP), degree of linear polarization (DOLP), and the degree of circular polarization (DOCP), evaluated according to Eqs. (12), (13), and (14). In a similar manner, the angle ψ and the ellipticity ε, as of Eqs. (15) and (16), are depicted in Fig. (8). Error figures are reported in Table 1.

$$\mathrm{DOP} = \frac{\sqrt{s_1^2 + s_2^2 + s_3^2}}{s_0}, \tag{12}$$

$$\mathrm{DOLP} = \frac{\sqrt{s_1^2 + s_2^2}}{s_0}, \tag{13}$$

$$\mathrm{DOCP} = \frac{\sqrt{s_3^2}}{s_0} = \frac{|s_3|}{s_0}, \tag{14}$$

$$\tan(2\psi) = \frac{s_2}{s_1}, \tag{15}$$

$$\sin(2\varepsilon) = \frac{s_3}{\sqrt{s_1^2 + s_2^2 + s_3^2}}. \tag{16}$$

Fig. 9 Image acquired when the modulator is driven with 5 V.

Even if significant error figures are obtained at some orientations of the quarter-wave plate, the overall behavior of our PSA meets our expectations.

4.2 *Imaging Validation*

Imaging validation is conducted as in our previous work with a rank-3 polarimeter.[10] We consider a transparent sample made of three polarizer strips with different orientations. The sample is illuminated with a circularly polarized beam produced by 25 green light emitting diodes, a beam homogenizer, an interference filter, a polarizer, and a quarter-wave plate. Figure 9 depicts the image acquired for V=5 V. It proves to be a little noisy. Figure 10 reports the evaluation of the four Stokes parameters at 200 fps for a given orientation of the sample. It should be noted that the reference angle in our images is aligned along the vertical polarizer. s_0, corresponding to the total intensity, appears noisier than the image acquired for V=5 V. This may be due to the inversion process, since the system CN is rather high. s_1 and s_2 globally exhibit little noise and estimate the corresponding parameters as expected. s_3 is much noisier, rather in the background which should appear uniformly white. Therefore the estimation of the circular component, possible through

Table 1 Error figures. Please remember that the source power fluctuates within 0.9%. Error on polarization angle is only evaluated when linear polarization is significant.

Parameter	DOP	DOLP	DOCP	Polar. angle ψ	Ellipticity ε
max. |error| over the whole angular range	9.6%	4.4%	9.2%	$\approx 4^\circ$(see caption)	2.1 $^\circ$
max. |error| for lin. polarizations (0°and 180°)	1.3%	1.3%	2.1%	0.7°	0.6 $^\circ$
max. |error| for circ. polarizations ($\pm$45°)	4.7%	3.6%	4.6%	–	1.0 $^\circ$
max. |error| at $\pm$30°	3.2%	2.9%	5.3%	3.4 $^\circ$	1.4°

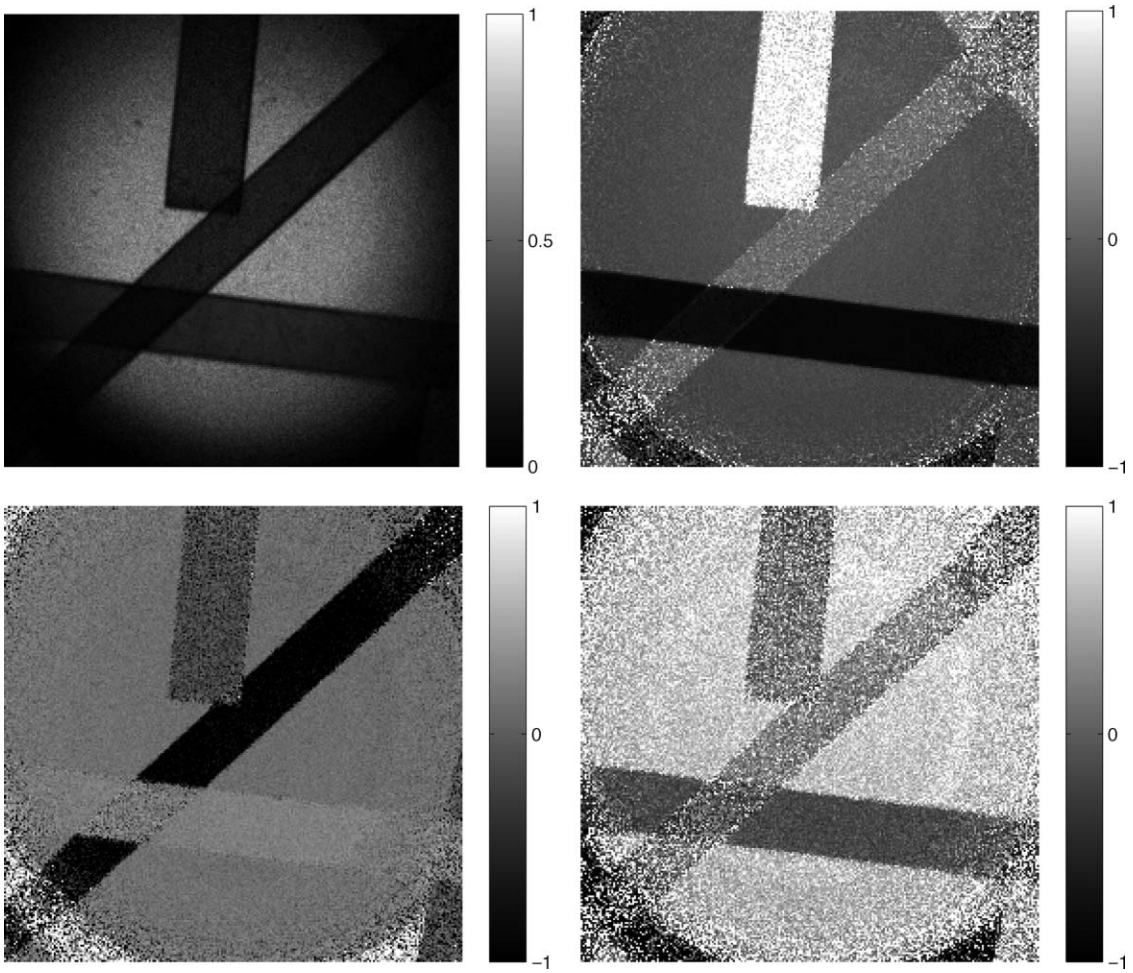

Fig. 10 Evaluation of the Stokes parameters of the test scene. From left to right and top to bottom: s_0, s_1/s_0, s_2/s_0, s_3/s_0.

the shift in wavelength, is not as good as the estimation of the other components.

Figure 11 reports the degree of linear polarization, the polarization angle, and the ellipticity. Linear polarization and polarization angle are correctly estimated, with only a little degradation compared to our implementation with three Stokes components.[10] Ellipticity, which could not be evaluated with our previous setup, is globally well estimated, with a strong difference between the polarizing strips and the background.

5 Discussion

The above reported experimental results clearly prove that using a single liquid crystal cell as the key part of a full Stokes polarization state analyzer is feasible. Nevertheless, the performance of our implementation remains lower from that of a laboratory precision setup. To improve such a setup, several ways could be considered. First, the condition number value, here 36.2, appears high, rather if we compare to our previous implementation concerning only linear polarization (CN was 4.2 in that case), or for instance to that reported in Ref. 16,

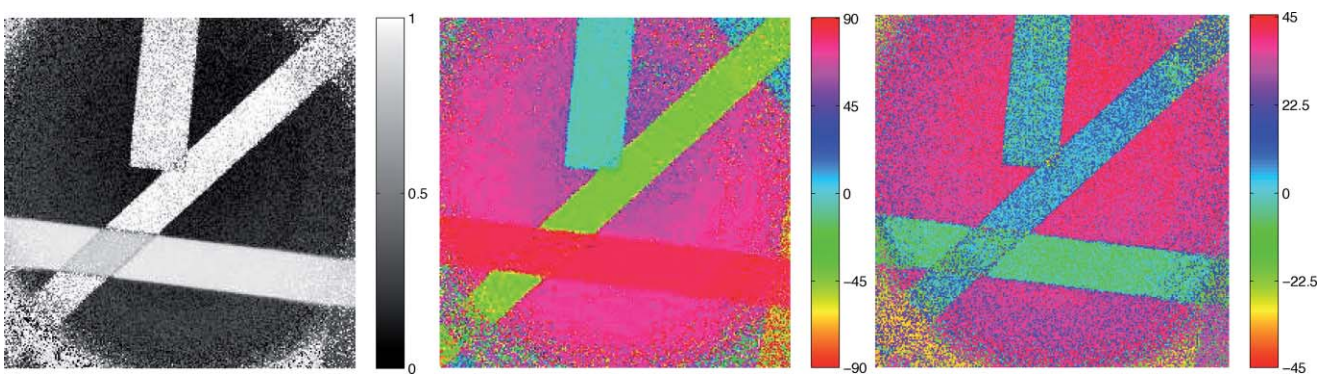

Fig. 11 From left to right: DOLP, angle of polarization ψ and ellipticity ϵ.

which provides a CN smaller than 2. Clearly, using an additional driving voltage in this case leads to a severe decrease in the condition number. This means that actually, with this kind of LC cell, decoupling the fast-axis orientation from the retardance remains difficult. The alternative consists of using two LC cells, as Gandorfer[9] and Vedel et al.,[17] but we wanted to avoid this solution, whose performance in terms of CN are not reported in previously cited references. In the present configuration, with two pairs of driving voltages instead of one during the characterization process, the nonlinear time-variant behavior of the modulator appears clear and further work shall be performed from the initial characterization. Using driving voltages outside the stable zone, i.e., between -1 and 3 V, is necessary to reduce the condition number, but makes the initial harmonic characterization only a starting point. Actually, an experimental iterative process should be considered in order to determine the best driving voltages. Furthermore, in this case, the transient driving pulse could probably be optimized.

Second, we have no temperature control of the PSA. A rather simple improvement would consist not in a temperature control, but in a compensation of the temperature induced phenomena, as proposed by Terrier et al.[18]

6 Conclusion

Imaging polarimetry has been challenging the optical community for 20 years as far as dynamic implementations are considered. Beside multi-channel configurations requiring dedicated highly optimized polarization modulating elements, division-of-time architectures using liquid crystal devices prove to be interesting alternatives, even if speeds higher than 100 fps are considered.

In this paper, we demonstrate the point in using a single analog ferroelectric liquid crystal modulator. Used at its nominal wavelength, such a device acts as a polarization rotator and cannot provide us information about circular polarization. Used away from its nominal wavelength, it behaves simultaneously as a rotator and an ellipticizer and can provide information about circular polarization, therefore allowing the user to retrieve full polarimetric information. Our portable implementation makes it possible to get full Stokes information at 200 fps. Since the polarimetric head only consists of a LC cell, a linear polarizer, and an interference filter, it can easily be considered for embedded applications.

References

1. G. G. Stokes, "On the composition and resolution of streams of polarized light from different sources," *Trans. Cambridge Philos. Soc.* **9**, 339–416 (1852).
2. R. Walraven, "Polarization imagery," in *Optical Polarimetry: Instrumentation and Applications, Proc. SPIE* **A79-11951 02-35**, 164–167 (1977).
3. J. Solomon, "Polarization imaging," *Appl. Opt.* **20**, 1537–1544 (1981).
4. R. A. Chipman, "*Polarimetry*," Chap. 22 in Handbook of Optics II, 2nd ed., M. Bass, Ed., McGraw-Hill, New York (1995).
5. S. Krishnan and P. C. Nordine, "Fast ellipsometry and mueller-matrix ellipsometry using the division-of-amplitude photopolarimeter," *Proc. SPIE* **2873**, 152–156 (1996).
6. E. de Leon, R. Brandt, A. Phenis, and M. Virgen, "Initial results of a simultaneous stokes imaging polarimeter," in *Polarization Science and Remote Sensing III, Proc. SPIE* **6682**, 668215 (2007).
7. F. A. Sadjadi and C. S. L. Chun, "Remote sensing using passive infrared stokes parameters," *Opt. Eng.* **43**, 2283–2291 (2004).
8. L. B. Wolff, T. A. Mancini, P. Pouliquen, and A. G. Andreou, "Liquid crystal polarization camera," *IEEE Trans. Rob. Autom.* **13**(2), 195–203 (1997).
9. A. M. Gandorfer, "Ferroelectric retarders as an alternative to piezoelastic modulators for use in solar stokes vector polarimetry," *Opt. Eng.* **38**, 1402–1408 (1999).
10. L. Gendre, A. Foulonneau, and L. Bigué, "Imaging linear polarimetry using a single ferroelectric liquid crystal modulator," *Appl. Opt.* **49**(25), 4687–4699 (2010).
11. S. L. Blakeney, S. E. Day, and J. N. Stewart, "Determination of unknown input polarisation using a twisted nematic liquid crystal display with fixed components," *Opt. Commun.* **214**, 1–8 (2002).
12. J. M. Bueno, "Polarimetry using liquid-crystal variable retarders: theory and calibration," *J. Opt. A; Pure App. Opt.* **2**, 216–222 (2000).
13. F. Goudail, P. Terrier, Y. Takakura, L. Bigué, F. Galland, and V. Devlaminck, "Target detection with a liquid crystal-based passive stokes polarimeter," *Appl. Opt.* **43**(2), 274–282 (2004).
14. D. Gisler, A. Feller, and A. Gandorfer, "Achromatic liquid crystal polarization modulator," in *Polarimetry in Astronomy, Proc. SPIE* **4843**, 45–54 (2003).
15. J. Scott Tyo, "Design of optimal polarimeters: maximization of signal-to-noise ratio and minimization of systematic error," *Appl. Opt.* **41**(4), 619–630 (2002).
16. P. Terrier, J. M. Charbois, and V. Devlaminck, "Fast-axis orientation dependence on driving voltage for a stokes polarimeter based on concrete liquid-crystal variable retarders," *Appl. Opt.* **49**(22), 4278–4283 (2010).
17. M. Vedel, N. Lechocinski, and S. Breugnot, "Compact and robust linear stokes polarization camera," in *Nanocharm Workshop, EPJ Web of Conferences* **5**, 01005 (2010).
18. P. Terrier, J. M. Charbois, and V. Devlaminck, "System and method for partial lcvr stokes polarimeter thermal drift compensation," in *Nanocharm Workshop, EPJ Web of Conferences* **5**, 01004 (2010).

Luc Gendre is a PhD student at Université de Haute Alsace. He graduated from the ECE Department at Université de Haute Alsace in 2007 after undergraduate studies in Aix-en-Provence. His research interests focus on high-speed imaging polarimetry, both on instrumental aspects (use of high-speed liquid crystal light modulators) and on image processing techniques (post-processing of polarimetric video sequences of moving objects). He is a member of SFO and EOS.

Alban Foulonneau received his engineering degree at the ENSPS (French College of Physics, Strasbourg, France) as well as his post-graduate degree in image processing, computer vision, and photonics at the Université de Strasbourg in 2001. He obtained a PhD in image processing and computer vision at the Université de Strasbourg in 2004. He has been an assistant professor at IUT de Mulhouse (College of Technology of Université de Haute Alsace, Mulhouse, France) since 2006. His major interests include computer vision and imaging polarimetry. He is a member of SFO and EOS.

Laurent Bigué received his engineering degree at the ENSPS (French College of Physics, Strasbourg, France) as well as his post-graduate degree in photonics and microelectronics at the Université de Strasbourg, in 1992. He obtained a PhD in optical, electrical, and computer engineering at the Université de Haute Alsace in 1996. He was appointed assistant professor at ENSISA (ECE Department of Université de Haute Alsace, Mulhouse, France) in 1998 and has been a professor at ENSISA since 2005. His major interests include optical signal processing, polarimetry, and optical metrology. He is a member of SFO, EOS, OSA and SPIE.